



Article

CuZr Metal Glass Powder as Electrocatalysts for Hydrogen and Oxygen Evolution Reactions

Zhangyu Xie ¹, Zhaoqi Song ², Jie Zhao ², Ying Li ², Xingke Cai ² , Dongqing Liu ^{1,*}, Jun Shen ¹ and Panagiotis Tsiakaras ³ 

¹ College of Mechatronics and Control Engineering, Shenzhen University, Shenzhen 518060, China

² Institute for Advanced Study, Shenzhen University, Shenzhen 518060, China

³ Laboratory of Alternative Energy Conversion Systems, Department of Mechanical Engineering, School of Engineering, University of Thessaly, 1 Sekeri Str., 38834 Volos, Greece

* Correspondence: liu.dongqing@szu.edu.cn

Abstract: For the practical application of water electrolysis, it is essential to develop cost-effective and high efficiency electrocatalysts for both hydrogen evolution reaction (HER) and oxygen evolution reaction (OER). In this work, we applied CuZr metallic glass powder, after chemical dealloying treatment, as electrocatalysts. The as-prepared sample had both the increased specific area and optimized surface composition of an efficient catalyst. During the HER and OER processes, the dealloyed CuZr sample displayed overpotential of 195 mV and 310 mV at current density of 10 mA cm⁻², respectively. A two-electrode water splitting cell, using the as-prepared CuZr sample, exhibited high stability towards a high current density of 500 mA cm⁻², and lower overpotential, compared to a Pt/C//IrO₂ cell, during the 10 mA cm⁻² constant current density aging test.

Keywords: hydrogen evolution reaction; oxygen evolution reaction; metallic glass



Citation: Xie, Z.; Song, Z.; Zhao, J.; Li, Y.; Cai, X.; Liu, D.; Shen, J.; Tsiakaras, P. CuZr Metal Glass Powder as Electrocatalysts for Hydrogen and Oxygen Evolution Reactions. *Catalysts* **2022**, *12*, 1378. <https://doi.org/10.3390/catal12111378>

Academic Editor: Nicolas Alonso-Vante

Received: 23 September 2022

Accepted: 5 November 2022

Published: 7 November 2022

Publisher's Note: MDPI stays neutral with regard to jurisdictional claims in published maps and institutional affiliations.



Copyright: © 2022 by the authors. Licensee MDPI, Basel, Switzerland. This article is an open access article distributed under the terms and conditions of the Creative Commons Attribution (CC BY) license (<https://creativecommons.org/licenses/by/4.0/>).

1. Introduction

The demand for renewable energy is urgent, due to the shortage of traditional energy sources, such as fossil fuels [1,2]. Various renewable energy sources have been developed, among which electrochemical water splitting is a high-efficiency and cost-effective method to produce hydrogen [3–5]. The water splitting reaction involves two reactions, i.e., hydrogen evolution reaction (HER) and oxygen evolution reaction (OER). As the HER and OER require high overpotentials to drive the reactions, various efficient electrocatalysts have been developed to boost the reaction efficiency [6–10]. Well-developed catalysts are usually costly, containing noble metals, such as Pt-based materials, Ru and Ir oxides. Thus, developing high efficiency electrocatalysts using cost-effective earth abundant elements is imperative for practical application.

Recently, research interests have been aroused in the application of amorphous alloys in water electrolysis as catalysts [11,12]. This is because of their unique atomic structure and high electrocatalytic activity, through nanostructure engineering, to produce high surface area [13]. Various metallic glass (MG)-based electrocatalysts have been applied in HER/OER or water electrolysis application, including noble metals containing IrNiTa [14,15], PdNiCuP [16], PtCuNiP [13,17], and PdPtCuNiP [18], and non-noble metals containing FeNiCo [19], NiFeP [20,21], FeCoPC [22], FeNiCoPC [23], etc. Most of the reports on this have utilized the self-standing ribbon form of the metallic glass and realized nanoengineering via chemical dealloying [15–18] or surface decoration [24]. Noteworthy, the rational design of high-efficiency metallic glass with non-noble metals is necessary for its practical application.

Here in this work, CuZr powder was treated with different concentrations of HF solutions for the chemical dealloying process. The as-prepared CuZr samples displayed different surface morphologies and compositions. Among the CuZr samples, CuZr–3* had

the largest surface area with a petal-like morphology and Cu oxides covering the surface. This ensured that CuZr-3* presented the best HER/OER performance among the CuZr samples and even had more superior OER activity than IrO₂. When coupled into the water electrolysis cell, the CuZr-3* cell showed good stability in the high current density and chronopotentiometry test.

2. Results and Discussion

2.1. Material Characterization

The morphology of the serial dealloyed samples, treated in different concentrations of HF solutions were observed by SEM. In Figure 1a of the CuZr-1 sample, the powders displayed 40–50 μm sized spherical morphology. After 0.1 M HF treatment, the surface cracked into 2–5 μm irregular flakes with 0.1–0.2 μm in between, adhering to the surface. In this case, the selective etching of CuZr by the HF solutions was minimal, and hardly met the expected effects. Figure 1b shows the CuZr-2 sample after 0.2 M HF treatment, the cracks on the surface of the spheres had almost disappeared. In contrast, the surface was covered with honeycomb-like holes from the local enlarged image of the spheres. Even through the surface area of CuZr-2 had increased, compared to that of CuZr-1, it was not obvious enough.

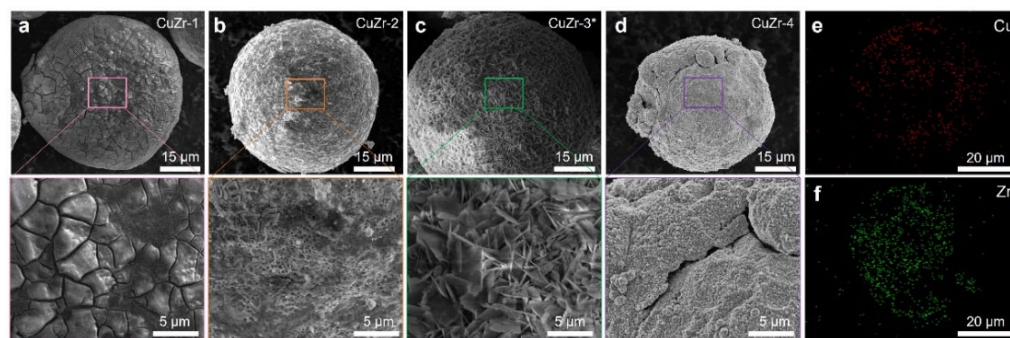


Figure 1. SEM images of the CuZr samples (a) CuZr-1; (b) CuZr-2; (c) CuZr-3*; and (d) CuZr-4. The EDS patterns of the CuZr-3* sample: (e) Cu and (f) Zr.

Figure 1c shows the CuZr-3* after 0.5 M HF treatment. A petal-like morphology with vertically aligned flakes had grown on the surface. Compared with the other two samples, the surface area of CuZr-3* had increased greatly. In this condition, the electrode/electrolyte contact area and exposure of reactive sites had increased, which was expected to enhance the electrocatalytic performance of CuZr-3*. In Figure 1d, when the HF concentration further increased to 1.0 M, the surface of CuZr-4 was etched and dissolved severely in the relatively concentrated 1 M HF solution. The spherical diameter of the CuZr-4 sample was obviously reduced, compared with the first three samples, and its surface was covered with loosely pulverized particles, which could easily dissolve after contact with the electrolyte. From the EDS mapping of CuZr-3*, the atomic ratio of copper to zirconium of the CuZr sample changed from the original 1:1 to 2:1 in the semi-quantitative analysis. This indicated selective dissolution of element Zr during the dealloying process, which agreed with previous reports [25,26].

The chemical composition and crystal structure were further characterized by XRD and XPS. According to the XRD patterns of the CuZr samples, as seen in Figure 2a, they could roughly be indexed into Cu, Cu₂O and CuO, but with different proportions. The pristine CuZr demonstrated the typical broad peak of metallic glass and sharp peaks corresponding to the Cu₂O/CuO species. This indicated the partial oxidation of the pristine CuZr powder during storage. Similarly, the CuZr-1 and CuZr-2 samples had much higher proportions of Cu₂O and CuO without the broad metallic glass peak. The CuZr-3* sample also displayed the Cu peaks, in addition to the CuO/Cu₂O species.

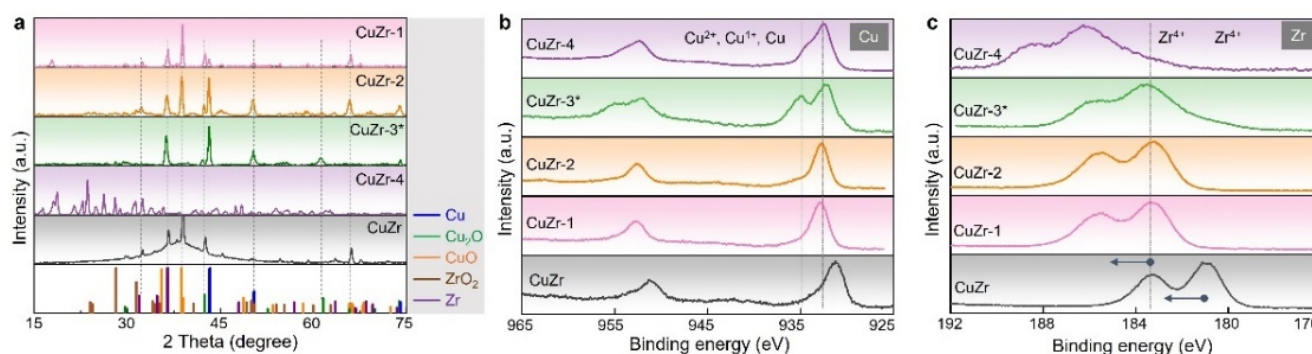


Figure 2. (a) XRD patterns of the dealloyed samples of CuZr alloy. (b) XPS spectra of (b) Cu 2p and (c) Zr 3d.

According to the XPS spectra of Cu 2p in Figure 2b, the CuZr-3* exhibited more intensified Cu^{2+} and Cu^{1+} peaks than the pristine CuZr sample. While for Zr 3d, in Figure 2c, the intensity of the Zr peaks was more reduced than at the pristine state, demonstrating the selective etching of the Zr element. The Zr peaks of CuZr at pristine state shifted towards higher oxidation states after dealloying to compensate for the charge imbalance. Therefore, the CuZr-3* sample, with its much larger specific surface covered by copper oxides CuO/Cu₂O, on exposure of the Cu surface after dealloying, was expected to show high HER/OER catalytic activity.

2.2. HER/OER Performance and Water Splitting Reaction

The electrocatalytic activity towards HER was examined by the LSV curves in Figure 3a. The as-prepared CuZr samples were compared with that of Cu foil and Pt/C. For the CuZr samples, the CuZr-3* displayed higher HER catalytic activity than the CuZr-4, CuZr-2, CuZr-1 and pristine CuZr, as expected. This could be evidenced more clearly by the overpotential values at 10 mA cm^{-2} , which were 242 mV, 215 mV, 195 mV and 206 mV, from CuZr-1 to CuZr-4 (Figure 3b). These CuZr samples were clearly much more active than the plain Cu foil with η_{10} of 496 mV, but they were hardly comparable with the commercial catalyst Pt/C, which had η_{10} only of 54 mV. The superb HER performance of the CuZr samples over the Cu foil was ascribed to the synergistic effect between copper zirconium glass alloy and copper oxides in improving catalytic activity [27].

The corresponding Tafel slopes are plotted in Figure 3c. The smaller the slope, the faster the reaction kinetics [28–30]. In accordance with the LSVs, the CuZr-3* sample displayed a Tafel slope of 92.8 mV dec^{-1} , lower than the 139, 101, and 95.3 mV dec^{-1} of CuZr-1, CuZr-2 and CuZr-4, but higher than the 60.8 mV dec^{-1} of Pt/C. Among the CuZr samples, the high catalytic activity and fast reaction kinetics of CuZr-3* should be beneficial, given the much larger exposure area of the reactive sites and facilitated charge/mass transfer process. This could be verified by the electrochemical surface area (ECSA) measurements in Figure 3d,e. As shown in Figure 3f, the CuZr-3* sample with a double layer capacitance C_{dl} value of 1.12 mF cm^{-2} had larger ECSAs than all the other CuZr samples. The reaction kinetics could be evidenced more clearly by the EIS measurement and corresponding equivalent circuit fitting.

Figure 3g shows the Nyquist plots of the CuZr samples individually measured at their η_{10} values. Through the equivalent fitting in Figure 3h, CuZr-3* displayed the lowest charge transfer resistance R_{ct} of 16Ω , lower than the 23, 35 and 41Ω of CuZr-1, CuZr-2 and CuZr-4, respectively. This verified the enhanced reaction kinetics of CuZr-3*, as discussed in [31]. The electrochemical stability of the CuZr-3* was further examined by measuring the LSV curves before and after the accelerated aging 1000 cycles CV test. In Figure 3i, the aged LSV curve nearly overlaps with the initial one, indicating the superior structural and electrocatalytic stability of the as prepared CuZr-3* sample.

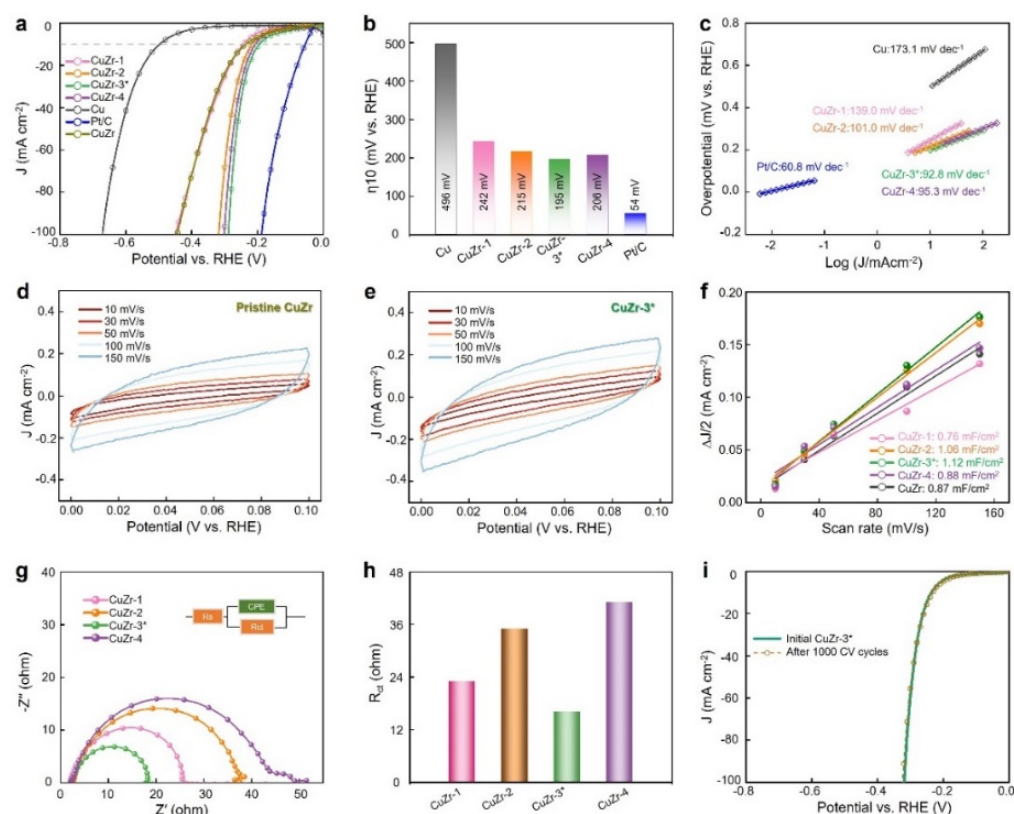


Figure 3. HER performance. (a) LSVs of the serial CuZr samples, Cu foil and Pt/C. The corresponding (b) overpotentials at 10 mA cm^{-2} and (c) Tafel slopes. (d,e) CV curves from 10 to 150 mV s^{-1} for the pristine and CuZr-3* samples. (f) The dependence of capacitive current densities with scan rates. (g) The Nyquist plots measured at the potentials corresponding to 10 mA cm^{-2} . (h) The fitted value of R_{ct} for each sample. (i) The LSVs of CuZr-3* before and after accelerated durability test.

Figure 4 shows the OER performance of the CuZr samples in comparison with Cu foil, Ni foam and IrO_2 . It was interesting to find that the serial CuZr displayed even better OER activity than the IrO_2 from the LSV curves in Figure 4a.

According to their overpotentials at 10 mA cm^{-2} (Figure 4b), the CuZr-1, CuZr-2 and CuZr-3 exhibited η_{10} values of 340 mV, 350 mV and 310 mV, lower than the 374 mV of IrO_2 , 380 mV of CuZr-4, and 538 mV of Cu foil. The superb performance of CuZr-1 to CuZr-3 indicated the positive role of CuZr alloy in supporting surface Cu oxides in boosting the OER catalytic activity [7,32,33]. It was noticed that there was an oxidation peak between 1.2 and 1.5 V from the LSV curve of each sample, except that of Cu foil. This was because the oxidation of foam nickel was exposed to alkaline electrolyte when the ink did not cover its whole surface [34]. The bare Ni foam sample was also tested for reference. In addition, the Tafel slopes and impedance spectra were used to analyze the reaction kinetics. In Figure 4c, the CuZr samples showed low Tafel slope values of 55.4 (CuZr-3*), 80.9 (CuZr-1), 82.8 (CuZr-2) and 88.6 mV dec^{-1} (CuZr-4), lower than that of IrO_2 , Ni foam or Cu foil.

The lowest Tafel slope of CuZr-3* verified its excellent surface morphology in increasing the reactive area and improving charge transfer. According to Figure 4d–f, the ECSA value derived from the C_{dl} was 220 cm^2 for the CuZr-3* sample, much larger than any of the CuZr samples. The Nyquist plots of the four CuZr samples, and their fitted values of R_{ct} , are shown in Figure 4g,h. In accordance with the Tafel slope, CuZr-3* had the lowest R_{ct} of 8.6Ω , lower than the 12.5Ω of CuZr-1, 12.9Ω of CuZr-2 and 16.7Ω of CuZr-4. This indicated that, with identical surface composition, the higher the surface exposure area, the faster the reaction rate. Furthermore, the accelerated aging tests result is shown in Figure 4i. After 1000 CV cycles, the OER activity of the CuZr-3* sample became even

better, which could be because of the partial dissolution of zirconium oxide in the alkaline solution further increasing the reactive surface area.

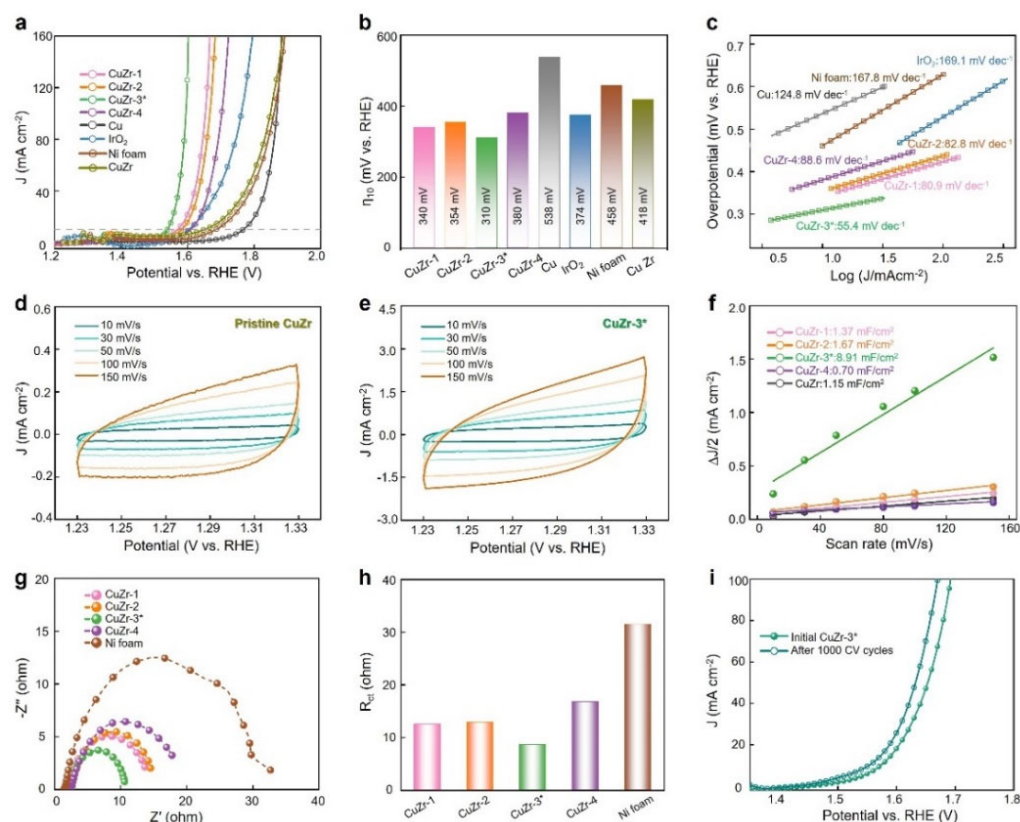


Figure 4. OER performance. (a) LSVs of the serial CuZr samples, Cu foil, Ni foam and IrO₂. The corresponding (b) overpotentials at 10 mA cm^{−2} and (c) Tafel slopes. (d,e) CV curves from 10 to 150 mV s^{−1} for the pristine and CuZr-3* samples. (f) The dependence of capacitive current densities with scan rates. (g) The Nyquist plots measured at the potentials corresponding to 10 mA cm^{−2}. (h) The fitted value of R_{ct} for each sample. (i) The LSVs of CuZr-3* before and after accelerated durability test.

To further examine the possibility for practical application, CuZr-3* electrodes, as cathode and anode, were assembled into the two-electrode configuration (inset of Figure 5a) for water electrocatalytic tests. The CuZr-3* sample was selected, as it best displayed HER and OER performance among the CuZr samples. According to Figure 5a, the CuZr-3*/CuZr-3* cell exhibited inferior catalytic activity than the Pt/C//IrO₂ cell but was obviously superior to the CuZr-3*/Ni foam cell. At a current density of 50 mA cm^{−2}, the overpotential of the Pt/C//IrO₂ cell was 530 mV, slightly lower than the 580 mV of the CuZr-3* cell. It is worth noticing that the CuZr-3* could sustain an ultra-high current density of 500 mA cm^{−2}, which demonstrated the structural and compositional stability of the CuZr-3* sample.

Additionally, a stability test was conducted through chronopotentiometry curves at constant current density of 10 mA cm^{−2}, shown in Figure 5b. The superiority of the CuZr-3* was demonstrated in this condition. The CuZr-3* cell displayed overpotential of 680 mV lasting for the more than 18 h, in contrast to the 820 mV of Pt/C//IrO₂ cell, even though its initial overpotential was much lower.

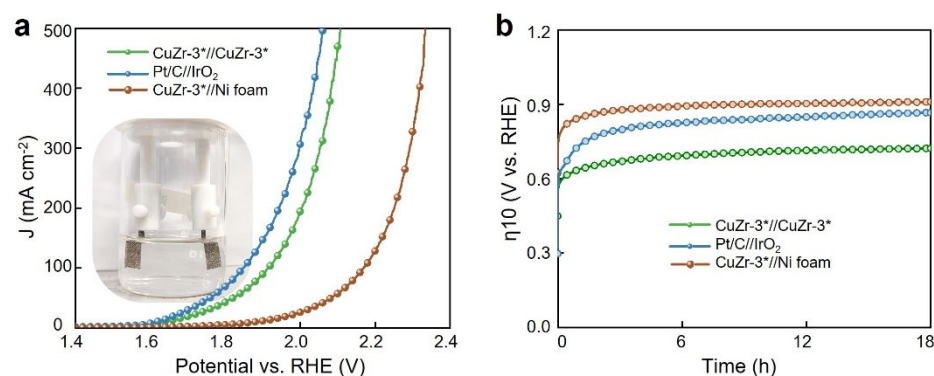


Figure 5. Water splitting reaction. (a) The LSV curves of Pt/C//IrO₂, CuZr-3*/CuZr-3* and CuZr-3*/Ni foam cells. (b) The chronopotentiometry curves of the two cells measured at applied current density of 10 mA cm⁻².

3. Experimental Section

3.1. Materials Preparation and Dealloying Treatment

The powder of copper zirconium metallic glass (Cu_{51.5}Zr_{48.5}, CuZr) was purchased from Panxing New Alloy Materials Co., Ltd. (Changzhou, China). The 20% Pt/C was obtained from Suzhou Sinero Technology Co., Ltd. (Suzhou, China). The Nafion solution (5 wt%) was supplied by Shanghai Yueci Electronic Technology Co., Ltd. (Shanghai, China). The Potassium hydroxide (KOH) and iridium dioxide (IrO₂) were ordered from Shanghai Macklin Biochemical Co., Ltd. (Shanghai, China).

The raw CuZr MG powder was chemically dealloyed in a series of HF solutions, i.e., 0.1 mol L⁻¹, 0.2 mol L⁻¹, 0.5 mol L⁻¹ and 1.0 mol L⁻¹, in the PTFE container with 6 mL HF solution added. To ensure sufficient reaction, the powder contained HF solution was magnetic stirred for 24 h at room temperature. Afterwards, the dealloyed CuZr powder was collected, rinsed with deionized water three times, and centrifuged at 10,000 r min⁻¹ for 5 min. Then the CuZr powder was put in the refrigerator for 6 h and dried with a freeze dryer. The as-prepared samples were named CuZr-1, CuZr-2, CuZr-3* and CuZr-4, corresponding to the four dealloying electrolytes.

3.2. Material Characterization

The amorphous structure of the MG samples was examined by X-ray diffractometer (XRD, Rigaku Corporation, Tokyo, Japan), using Cu K_α as the radiation source at 40 kV and 40 mA. The XRD pattern was obtained by scanning from 20° to 80° at a scan speed of 5-degree min⁻¹. The morphology and element mapping were analyzed by a scanning electron microscope (SEM, Thermo Scientific, Waltham, MA, USA) and an energy dispersive spectrometer (EDS).

3.3. Electrochemical Measurement

All electrochemical tests were carried out using electrochemical workstation of Chenhua (CHI760E) at room temperature of 25 °C. Three electrode and two electrode configurations were applied for HER/OER and water splitting tests, respectively. To prepare the working electrode of HER/OER, 5 mg of the dealloyed CuZr powder and 30 µL Nafion as the binder were dissolved in the solvent containing 700 µL deionized water and 300 µL isopropyl alcohol. Then, the obtained solution was stirred and ultrasonically treated for 30 min to prepare the electrode ink. Afterwards, 40 µL of the ink was dropped on the nickel foam (0.5 cm × 1 cm) evenly, displaying mass loading of 0.38 mg cm⁻², and dried under an infrared lamp for 20 min prior to use. The Pt/C and IrO₂ electrode preparation was the same as in our previous report [15]. For the copper electrode, the copper foil was cut into an area of 0.5 cm × 1 cm and applied as working electrode for comparison. For the three-electrode cell of HER, platinum foil (1.5 cm × 1.5 cm) was the counter electrode and Hg/HgO was used as the reference electrode. The measured potential was converted to the

reversible hydrogen electrode (RHE) for standard comparison via the following equation: $R_{RHE} = E_{H_2/H_2O} + 0.926$ V. All the electrochemical measurements were carried out in an alkaline solution of 1 M KOH.

During the HER measurements, the electrode was pre-activated and scanned by the cyclic voltammetry (CV) method at a scan rate of 100 mV s^{-1} until the CV curves were stable. Afterwards, the linear sweep voltammetry (LSV) test was performed in the potential range of -0.8 V to 0.0 V at a scan rate of 5 mV s^{-1} . The accelerated durability test (ADT) was carried out by CV scans between -0.8 V and 0.0 V for 1000 cycles at 100 mV s^{-1} . For OER, the LSV and ADT measurements followed the same procedure as HER but in the voltage range of 1.2 V to 2.0 V. The electrochemical impedance spectroscopy (EIS) was measured at an overpotential of each cell at 10 mA cm^{-2} in the frequency range of 100 kHz to 0.1 Hz and voltage amplitude of 5 mV . For the overall water splitting reaction, the LSV test was performed from 1.2 V to 2.1 V at a scanning speed of 5 mV s^{-1} . The stability test was carried out by chronopotentiometry at a constant current density of 10 mA cm^{-2} for 18 h.

4. Conclusions

The powder of CuZr metallic glass was chemically dealloyed in HF solution and applied as an electrocatalyst for HER, OER and water splitting reactions. The CuZr sample, dealloyed in 0.5 mol L^{-1} solution for 24 h, displayed an enlarged surface area with petal-like morphology and copper oxide coverage. It displayed inferior HER performance than the commonly used Pt/C but superior OER activity than the commercial IrO_2 . This work presents a simple and effective method to activate low cost CuZr MG powder for practical application in electrocatalysis.

Author Contributions: Methodology: Z.X., Z.S. and J.Z.; formal analysis: Z.X., J.Z. and Y.L.; data curation: Z.X., Z.S. and Y.L.; writing—original draft preparation: Z.X.; writing—review and editing: D.L. and P.T.; supervision: D.L., X.C. and J.S.; funding acquisition: D.L. All authors have read and agreed to the published version of the manuscript.

Funding: This work was supported by the Natural Science Foundation of China: No. 22105129; Guangdong Basic and Applied Basic Research Foundation: No. 2022A1515011048, NTUT-SZU Joint Research Program: No. 2022005.

Data Availability Statement: The data is available upon request from the corresponding author.

Conflicts of Interest: The authors declare no conflict of interest.

References

1. Li, Z.; Feng, H.; Song, M.; He, C.; Zhuang, W.; Tian, L. Advances in CoP electrocatalysts for water splitting. *Mater. Today Energy* **2021**, *20*, 100698. [\[CrossRef\]](#)
2. Najam, T.; Shah, S.S.A.; Ibraheem, S.; Cai, X.; Hussain, E.; Suleman, S.; Javed, M.S.; Tsiakaras, P. Single-atom catalysis for zinc-air/ O_2 batteries, water electrolyzers and fuel cells applications. *Energy Stor. Mater.* **2022**, *45*, 504–540. [\[CrossRef\]](#)
3. Wang, Y.; Liu, B.; Shen, X.; Arandiyana, H.; Zhao, T.; Li, Y.; Garbrecht, M.; Su, Z.; Han, L.; Tricoli, A.; et al. Engineering the Activity and Stability of MOF-Nanocomposites for Efficient Water Oxidation. *Adv. Energy Mater.* **2021**, *11*, 2003759. [\[CrossRef\]](#)
4. Lin, Z.; Liu, S.; Liu, Y.; Liu, Z.; Zhang, S.; Zhang, X.; Tian, Y.; Tang, Z. Rational design of Ru aerogel and RuCo aerogels with abundant oxygen vacancies for hydrogen evolution reaction, oxygen evolution reaction, and overall water splitting. *J. Power Sources* **2021**, *514*, 230600. [\[CrossRef\]](#)
5. Nguyen, D.C.; Luyen Doan, T.L.; Prabhakaran, S.; Tran, D.T.; Kim, D.H.; Lee, J.H.; Kim, N.H. Hierarchical Co and Nb dual-doped MoS_2 nanosheets shelled micro- TiO_2 hollow spheres as effective multifunctional electrocatalysts for HER, OER, and ORR. *Nano Energy* **2021**, *82*, 105750. [\[CrossRef\]](#)
6. Vij, V.; Sultan, S.; Harzandi, A.M.; Meena, A.; Tiwari, J.N.; Lee, W.-G.; Yoon, T.; Kim, K.S. Nickel-Based Electrocatalysts for Energy-Related Applications: Oxygen Reduction, Oxygen Evolution, and Hydrogen Evolution Reactions. *ACS Catal.* **2017**, *7*, 7196–7225. [\[CrossRef\]](#)
7. Gao, J.; Yang, L.; Wang, D.; Cao, D. Hollow Nanotube $\text{Ru/Cu}_{24}\text{O}$ Supported on Copper Foam as a Bifunctional Catalyst for Overall Water Splitting. *Chem. Eur. J.* **2020**, *26*, 4112–4119. [\[CrossRef\]](#)

8. Cui, S.; Li, M.; Bo, X. Co/Mo₂C composites for efficient hydrogen and oxygen evolution reaction. *Int. J. Hydrog. Energy* **2020**, *45*, 21221–21231. [\[CrossRef\]](#)
9. Zhu, Y.; Zhou, W.; Zhong, Y.; Bu, Y.; Chen, X.; Zhong, Q.; Liu, M.; Shao, Z. A Perovskite Nanorod as Bifunctional Electrocatalyst for Overall Water Splitting. *Adv. Energy Mater.* **2017**, *7*, 1602122. [\[CrossRef\]](#)
10. Najam, T.; Ibraheem, S.; Nazir, M.A.; Shaheen, A.; Waseem, A.; Javed, M.S.; Shah, S.S.A.; Cai, X. Partially oxidized cobalt species in nitrogen-doped carbon nanotubes: Enhanced catalytic performance to water-splitting. *Int. J. Hydrog. Energy* **2021**, *46*, 8864–8870. [\[CrossRef\]](#)
11. Li, X.; Cai, W.; Li, D.-S.; Xu, J.; Tao, H.; Liu, B. Amorphous alloys for electrocatalysis: The significant role of the amorphous alloy structure. *Nano Res.* **2021**, 1–12. [\[CrossRef\]](#)
12. Jiang, R.; Da, Y.; Chen, Z.; Cui, X.; Han, X.; Ke, H.; Liu, Y.; Chen, Y.; Deng, Y.; Hu, W. Progress and Perspective of Metallic Glasses for Energy Conversion and Storage. *Adv. Energy Mater.* **2022**, *12*, 2101092. [\[CrossRef\]](#)
13. Carmo, M.; Sekol, R.C.; Ding, S.; Kumar, G.; Schroers, J.; Taylor, A.D. Bulk Metallic Glass Nanowire Architecture for Electrochemical Applications. *ACS Nano* **2011**, *5*, 2979–2983. [\[CrossRef\]](#) [\[PubMed\]](#)
14. Wang, Z.-J.; Li, M.-X.; Yu, J.-H.; Ge, X.-B.; Liu, Y.-H.; Wang, W.-H. Low-Iridium-Content IrNiTa Metallic Glass Films as Intrinsically Active Catalysts for Hydrogen Evolution Reaction. *Adv. Mater.* **2020**, *32*, 1906384. [\[CrossRef\]](#) [\[PubMed\]](#)
15. Liu, D.; Song, Z.; Cheng, S.; Wang, Y.; Saad, A.; Deng, S.; Shen, J.; Huang, X.; Cai, X.; Tsiakaras, P. Mesoporous IrNiTa metal glass ribbon as a superior self-standing bifunctional catalyst for water electrolysis. *Chem. Eng. J.* **2022**, *431*, 134210. [\[CrossRef\]](#)
16. Hu, Y.C.; Wang, Y.Z.; Su, R.; Cao, C.R.; Li, F.; Sun, C.W.; Yang, Y.; Guan, P.F.; Ding, D.W.; Wang, Z.L.; et al. A Highly Efficient and Self-Stabilizing Metallic-Glass Catalyst for Electrochemical Hydrogen Generation. *Adv. Mater.* **2016**, *28*, 10293–10297. [\[CrossRef\]](#) [\[PubMed\]](#)
17. Doubek, G.; Sekol, R.C.; Li, J.; Ryu, W.-H.; Gittleston, F.S.; Nejati, S.; Moy, E.; Reid, C.; Carmo, M.; Linardi, M.; et al. Guided Evolution of Bulk Metallic Glass Nanostructures: A Platform for Designing 3D Electrocatalytic Surfaces. *Adv. Mater.* **2016**, *28*, 1940–1949. [\[CrossRef\]](#)
18. Jia, Z.; Nomoto, K.; Wang, Q.; Kong, C.; Sun, L.; Zhang, L.-C.; Liang, S.-X.; Lu, J.; Kruzic, J.J. A Self-Supported High-Entropy Metallic Glass with a Nanosponge Architecture for Efficient Hydrogen Evolution under Alkaline and Acidic Conditions. *Adv. Funct. Mater.* **2021**, *31*, 2101586. [\[CrossRef\]](#)
19. Jin, Y.; Xi, G.; Li, R.; Li, Z.-A.; Chen, X.-B.; Zhang, T. Nanoporous metallic-glass electrocatalysts for highly efficient oxygen evolution reaction. *J. Alloys Compd.* **2021**, *852*, 156876. [\[CrossRef\]](#)
20. Tan, Y.; Zhu, F.; Wang, H.; Tian, Y.; Hirata, A.; Fujita, T.; Chen, M. Noble-Metal-Free Metallic Glass as a Highly Active and Stable Bifunctional Electrocatalyst for Water Splitting. *Adv. Mater. Interfaces* **2017**, *4*, 1601086. [\[CrossRef\]](#)
21. Hu, F.; Zhu, S.; Chen, S.; Li, Y.; Ma, L.; Wu, T.; Zhang, Y.; Wang, C.; Liu, C.; Yang, X.; et al. Amorphous Metallic NiFeP: A Conductive Bulk Material Achieving High Activity for Oxygen Evolution Reaction in Both Alkaline and Acidic Media. *Adv. Mater.* **2017**, *29*, 1606570. [\[CrossRef\]](#) [\[PubMed\]](#)
22. Zhang, F.; Wu, J.; Jiang, W.; Hu, Q.; Zhang, B. New and Efficient Electrocatalyst for Hydrogen Production from Water Splitting: Inexpensive, Robust Metallic Glassy Ribbons Based on Iron and Cobalt. *ACS Appl. Mater. Interfaces* **2017**, *9*, 31340–31344. [\[CrossRef\]](#)
23. Aneeshkumar, K.S.; Tseng, J.-c.; Liu, X.; Tian, J.; Diao, D.; Shen, J. Electrochemically dealloyed nanoporous Fe₄₀Ni₂₀Co₂₀P₁₅C₅ metallic glass for efficient and stable electrocatalytic hydrogen and oxygen generation. *RSC Adv.* **2021**, *11*, 7369–7380. [\[CrossRef\]](#) [\[PubMed\]](#)
24. Yan, Y.; Wang, C.; Huang, Z.; Fu, J.; Lin, Z.; Zhang, X.; Ma, J.; Shen, J. Highly efficient and robust catalysts for the hydrogen evolution reaction by surface nano engineering of metallic glass. *J. Mater. Chem. A* **2021**, *9*, 5415–5424. [\[CrossRef\]](#)
25. Bae, J.-W.; Kim, M.-J.; Seo, J.-H. Wet Etching Behavior of Amorphous CuZr Thin Film in Hydrogen Peroxide Solution for Stretchable Display. *ECS J. Solid State Sci. Technol.* **2021**, *10*, 056005. [\[CrossRef\]](#)
26. Liu, D.; Wang, Y.; Tong, T.; Luo, G.; Shen, J.; Cai, X. Mesoporous copper-based metal glass as current collector for Li metal anode. *Chem. Eng. J.* **2023**, *451*, 138910. [\[CrossRef\]](#)
27. Avani, A.V.; Anila, E.I. Recent advances of MoO₃ based materials in energy catalysis: Applications in hydrogen evolution and oxygen evolution reactions. *Int. J. Hydrog. Energy* **2022**, *47*, 20475–20493. [\[CrossRef\]](#)
28. Jiang, S.; Zhu, L.; Yang, Z.; Wang, Y. Self-supported hierarchical porous FeNiCo-based amorphous alloys as high-efficiency bifunctional electrocatalysts toward overall water splitting. *Int. J. Hydrog. Energy* **2021**, *46*, 36731–36741. [\[CrossRef\]](#)
29. Li, Z.; Sui, J.; Zhang, Q.; Yu, J.; Yu, L.; Dong, L. CoP@NC electrocatalyst promotes hydrogen and oxygen productions for overall water splitting in alkaline media. *Int. J. Hydrog. Energy* **2021**, *46*, 2095–2102. [\[CrossRef\]](#)
30. Ouyang, C.; Wang, X.; Wang, C.; Zhang, X.; Wu, J.; Ma, Z.; Dou, S.; Wang, S. Hierarchically Porous Ni₃S₂ Nanorod Array Foam as Highly Efficient Electrocatalyst for Hydrogen Evolution Reaction and Oxygen Evolution Reaction. *Electrochim. Acta* **2015**, *174*, 297–301. [\[CrossRef\]](#)
31. Kumar, P.; Murthy, A.P.; Bezerra, L.S.; Martini, B.K.; Maia, G.; Madhavan, J. Carbon supported nickel phosphide as efficient electrocatalyst for hydrogen and oxygen evolution reactions. *Int. J. Hydrog. Energy* **2021**, *46*, 622–632. [\[CrossRef\]](#)
32. Chen, Y.; Cai, Z.; Wang, D.; Yan, Y.; Wang, P.; Wang, X. Air-Stable Mn doped CuCl/CuO Hybrid Triquetrous Nanoarrays as Bifunctional Electrocatalysts for Overall Water Splitting. *Chem. Asian J.* **2021**, *16*, 3107–3113. [\[CrossRef\]](#) [\[PubMed\]](#)

-
33. Liu, Q.; Liu, Q.; Kong, X. Cu-Based Nanosheet Arrays for Water-Splitting. *ACS Appl. Nano Mater.* **2019**, *2*, 6000–6009. [[CrossRef](#)]
 34. Saad, A.; Gao, Y.; Owusu, K.A.; Liu, W.; Wu, Y.; Ramiere, A.; Guo, H.; Tsiakaras, P.; Cai, X. Ternary Mo₂NiB₂ as a Superior Bifunctional Electrocatalyst for Overall Water Splitting. *Small* **2022**, *18*, 2104303. [[CrossRef](#)] [[PubMed](#)]